RESEARCH PAPERS

Acta Cryst. (1999). A**55**, 1–13

Nonsymmetrical X-ray diffraction in a perfect rectangular $t \times l$ crystal. Extinction and absorption

GUNNAR THORKILDSEN* AND HELGE B. LARSEN

Department of Mathematics and Natural Science, Stavanger College, Ullandhaug, 4004 Stavanger, Norway. E-mail: gunnar.thorkildsen@tn.his.no

(*Received 31 January 1998; accepted 3 April 1998*)

Abstract

A theoretical investigation of diffraction in a rectangular $t \times l$ crystal for nonsymmetrical coplanar scattering has been undertaken. The asymmetry in the scattering geometry, measured by an angle γ, causes different weights for the mixed Laue–Bragg contributions to the integrated power. Primary extinction and ordinary absorption are only moderately affected when the value of the geometrical parameter $\zeta = (t/l)\tan\theta_{oh} < 1$, θ_{oh} being the Bragg angle. For increasing values of ζ and γ the surface integration set-up for the Laue and Bragg regions is extensively changed, leading to pronounced effects. Analytical results for the normal absorption factor are presented.

1. Introduction

In a series of papers, we have addressed the topic of dynamical two-beam diffraction in finite perfect crystals. Both cylindrical and spherical (Thorkildsen & Larsen, 1998*a*,*b*) and parallelepipedal crystals (Thorkildsen & Larsen, 1998*c*) have been considered. For the latter case, hereafter denoted TL98*c*, a symmetrical scattering situation was adopted. In the present treatment, we seek to extend the formalism to comprise nonsymmetrical scattering conditions.

The principal mathematical approach, the boundary-value Green-function technique for solving the Takagi–Taupin equations (Takagi, 1962, 1969; Taupin, 1964), has been thoroughly outlined in the previous papers. This work gives the changes in the region geometry, the Green functions and the integration set-up caused by the diffraction asymmetry. The effect of the asymmetry on primary extinction and absorption is outlined. We only consider a coplanar scattering situation, *i.e.* the surface normals are parallel to the diffraction plane.

Standard treatment of nonsymmetrical diffraction in semi-infinite crystal plates, based on the fundamental theory of diffraction, is for instance found in chapter 4 in the book of Pinsker (1978). An extensive treatment on the subject, with particular emphasis on integrated reflectivity in the Bragg case, is due to Wilkins (1978, 1981). The surface integration approach that we use allows us to handle in principle any $t \times l$ cross section and corresponding allowed asymmetry. We have to point out, however, that the effects arising from specular reflections in the extreme asymmetrical limits are not covered by the present analysis. For an exact treatment in such a situation, the standard dynamical theory is to be modified (Afanasev & Melkonyan, 1983; Hung & Chang, 1989; Holý, 1996).

2. Theory

2.1. *General*

In TL98*c*, it is shown that the generalized extinction factor, y, and the normal absorption factor, A, for symmetrical scattering in a perfect $t \times l$ crystal can be expressed by†

$$y = (1/2\zeta)\sum_{\mathsf{s}}\sum_{m=m'(\zeta;\mathsf{s})}\int_{M(\zeta;m,\mathsf{s})}\mathrm{d}y\int_{S(y,\zeta;m,\mathsf{s})}\mathrm{d}x \times |G_h(\Delta_o, \Delta_h|m; r_{\mathsf{s}})|^2 \exp[-\mu_0(\Delta_o + \Delta_h)] \quad (1)$$

and

$$A = (1/2\zeta)\sum_{\mathsf{s}}\sum_{m=m'_0(\zeta;\mathsf{s})}\int_{M(\zeta;m,\mathsf{s})}\mathrm{d}y\int_{S(y,\zeta;m,\mathsf{s})}\mathrm{d}x \times \exp[-\mu_0(\Delta_o + \Delta_h)]. \quad (2)$$

These results are derived from the Takagi–Taupin equations (Takagi, 1962, 1969; Taupin, 1964):

$$\partial\tilde{D}_o/\partial s_o = i\kappa_{oh}\tilde{D}_h \quad (3)$$

$$\partial\tilde{D}_h/\partial s_h = i\kappa_{ho}\tilde{D}_o \quad (4)$$

using the point-source concept (Becker, 1977) and the Riemann–Green method (Sommerfeld, 1949). The entrance and exit surfaces are classified according to the crystal faces (A, B, C, D) and s labels the different combinations of positions for source (S) and exit (M) points. m covers the actual regions‡ at the exit for the

† In this work, we will not address anomalous scattering.

‡ In the case of normal absorption, this means only those regions that have a zeroth-order term (= 1) in the field expansion.

Table 1. *Dimensionless coordinates for a point M on an exit surface relative to a source point S*

Surfaces	Δ_o	Δ_h	c
A–A	$(\beta_+/\beta_-)x$	x	–
A–D	$(\beta_+/\beta_-)x + 2\beta_+\delta_- y$	x	–
B–A	$2\beta_-\delta_+ y - (\delta_+/\delta_-)x$	x	$2\delta_+ x - 2(\beta_-\delta_+/\beta_+)y$
B–D	$2\delta_+\zeta - (\delta_+/\delta_-)x$	x	$2\delta_+ x + 2\delta_- y - 2(\delta_+/\beta_+)\zeta$

Bragg and Laue families (r), *cf.* Figs. 1–4. Δ_o and Δ_h are the coordinates of the exit point relative to the source measured in a local coordinate system (s_o, s_h) with origin at S. The surface integrations are performed using sets of convenient variables (x, y). The geometrical quantity ζ is defined by

$$\zeta = (t/l)\tan\theta_{oh}, \tag{5}$$

where θ_{oh} is the Bragg angle. Furthermore, $\mu_0 = \mu\ell$ with μ the linear absorption coefficient. ℓ is the characteristic length parameter $l/(2\sin\theta_{oh})$. The coupling strength, κ_{pq}, is proportional to the Fourier expansion coefficient of the dielectric susceptibilty,† $\kappa_{pq} = -\pi K\chi_{p-q}C$. The families of functions $\{i\kappa_{ho}G_h(s_o, s_h|m; r)\}$ are the boundary-value Green functions, *i.e.* the solution of the Takagi–Taupin equations for the diffracted field using the boundary condition‡

$$\tilde{D}_o(S) = \delta(s_h). \tag{6}$$

The above concept is readily generalized to the case of nonsymmetrical scattering, which is parametrized using the asymmetry angle γ, *cf.* §2.2 and Fig. 1.

We have to search for:

(i) The Green functions: $G_h(s_o, s_h|\gamma)$.

(*a*) As a series:

$$G_h(s_o, s_h|\gamma) = \sum_{n=0}^{\infty}(-u)^n G_h^{(n)}(s_o, s_h|\gamma).$$

This approach focuses on the events of scattering–rescattering. It gives analytical results for the normal absorption factor and for the coefficients in a series for the extinction factor. The series found are slowly convergent, and the computational labour to obtain higher-order terms soon increases beyond practical limits. The expansion parameter u is defined by $u = \kappa_{oh}\kappa_{ho}\ell^2$ and its absolute value§ $|u| = (\ell/\Lambda_{oh})^2$, with $\Lambda_{oh} = 1/(|\kappa_{oh}\kappa_{ho}|)^{1/2}$ being an extinction length.

(*b*) In closed forms: these are obtained by applying the results of Uragami (1971). It then becomes possible to perform extensive numerical calculations.

(ii) The integration structure:

$$\int_{M(\gamma)} \mathrm{d}y \int_{S(\gamma)} \mathrm{d}x.$$

† All symbols have their standard interpretation.

‡ δ denotes the Dirac delta function.

§ u is in general a complex quantity owing to the effect of resonance scattering. That aspect is however not explored in this paper, *cf.* TL98*c*.

In this work, we stress the changes owing to the introduction of the asymmetry angle γ compared with the formalism covered in TL98*c*.

2.2. *Geometry*

The deviation from a symmetrical scattering condition is measured by the angle γ as shown in Fig. 1. Since we keep A and B as the entrance surfaces, the angle γ must satisfy the conditions

$$\text{if } 0 \le \theta_{oh} \le \pi/4 \quad \text{then} \quad -\theta_{oh} \le \gamma \le \theta_{oh} \tag{7}$$

$$\text{if } \pi/4 \le \theta_{oh} \le \pi/2 \quad \text{then} \quad \theta_{oh} - \pi/2 \le \gamma \le \pi/2 - \theta_{oh}. \tag{8}$$

In Fig. 2, we have shown the coordinate systems used in this calculation. The relations between the coordinates are explored in Appendix *A*.

In the subsequent treatment, we will use the definitions¶

$$\beta_\pm = \sin\theta_{oh}/\sin(\theta_{oh} \pm \gamma) \tag{9}$$

$$\delta_\pm = \cos\theta_{oh}/\cos(\theta_{oh} \pm \gamma). \tag{10}$$

The following relations exist between these quantities:

$$\beta_+/\delta_+ + \beta_-/\delta_- = 2\beta_+\beta_- \tag{11}$$

$$\delta_+/\beta_+ + \delta_-/\beta_- = 2\delta_+\delta_-. \tag{12}$$

All lengths will be measured in the characteristic length ℓ. Thus the area of the rectangular diffraction plane becomes $tl = 2\zeta\ell^2\sin 2\theta_{oh}$.

The Bragg and Laue families of regions are shown in Figs. 3 and 4. The expressions for Δ_o, Δ_h and $c = 2r_1(S)/l$ in the chosen coordinate representations, *cf.* Appendix *A*, are summarized in Table 1. Some of the more technical details that are introduced simplify the construction of *Mathematica*†† algorithms used for the calculations. The relations given cover the case of positive values of γ. The change to negative values of this parameter can be accomplished by an interchange of the $\pm$ indices.

¶ Compared with the notation of Authier (1996), we have $\beta_+/\beta_- = |\gamma_h|/\gamma_o$ in reflection geometry and $\delta_+/\delta_- = \gamma_h/\gamma_o$ in transmission geometry, $\gamma_o = \cos(\mathbf{n}, \mathbf{s}_o)$ and $\gamma_h = \cos(\mathbf{n}, \mathbf{s}_h)$ with $\mathbf{n}$ being the inward drawn normal vector to the actual crystal surface.

†† *Mathematica* is the trademark of Wolfram Research Inc., Champaign, IL 61820–7237, USA.

Table 2. *Defining integral operators for the Bragg family, $r = \mathsf{B}$, $p = 0, 1, \ldots$*

Region	$\mathcal{L}_{oh}$	$\mathcal{L}_{ho}$
$m = 2p+1$	$\int_{(\beta_+/\beta_-)s_h}^{s_o} \mathrm{d}s'_o$	$\int_{2p\beta_-}^{s_h} \mathrm{d}s'_h$
$m = 2p+2$	$\int_{2(p+1)\beta_+}^{s_o} \mathrm{d}s'_o$	$\int_{(\beta_-/\beta_+)s_o - 2\beta_-}^{s_h} \mathrm{d}s'_h$

2.3. *Field solutions*

2.3.1. *Series expansion*. The series-expansion coefficients for the boundary-value Green functions are given by a set of coupled recurrence relations, *cf.* equations (22) and (23) of TL98*c*. The integral operators $\mathcal{L}_{ho}$ and $\mathcal{L}_{oh}$ will depend on the degree of asymmetry and are given in Tables 2 and 3. Using the boundary conditions introduced in TL98*c*, it is straightforward to implement this procedure in *Mathematica* to calculate the coefficients $\{G_h^{(n)}\}$ to any practical order.

2.3.2. *Closed forms*. The boundary-value Green functions in each region can be expressed by recurrence relations too, one for the Laue family, another one for the Bragg family. The two sets of recurrence relations are identical to those of the symmetrical case and are given in equations (24)–(28) of TL98*c*.

The following definitions of functions apply to the nonsymmetrical case:

$$G_h(s_o, s_h|1; \mathsf{L}) = J_0[2(us_o s_h)^{1/2}] \tag{13}$$

$$G_h(s_o, s_h|1; \mathsf{B}) = J_0[2(us_o s_h)^{1/2}] + (\beta_+/\beta_-)(s_h/s_o) \times J_2[2(us_o s_h)^{1/2}] \tag{14}$$

$$w(s_o, s_h|6p+2; \mathsf{L}) = (-1)^p \left[\frac{\beta_+}{\beta_-}\frac{s_h - (2p+c)\beta_-}{s_o + (2p+c)\beta_+}\right]^{p+1} \times J_{2p+2}\big(2\{u[s_o + (2p+c)\beta_+][s_h - (2p+c)\beta_-]\}^{1/2}\big) \tag{15}$$

$$w(s_o, s_h|6p+3; \mathsf{L}) = (-1)^{p+1} \left\{\frac{\beta_-}{\beta_+}\frac{s_o - [(2p+2)-c]\beta_+}{s_h + [(2p+2)-c]\beta_-}\right\}^{p} \times J_{2p}\big[2\big(u\{s_o - [(2p+2)-c]\beta_+\} \times \{s_h + [(2p+2)-c]\beta_-\}\big)^{1/2}\big] \tag{16}$$

$$w(s_o, s_h|6p+5; \mathsf{L}) = (-1)^{p+1} \left[\frac{\beta_+}{\beta_-}\frac{s_h - (2p+2)\beta_-}{s_o + (2p+2)\beta_+}\right]^{p+1} \times J_{2p+2}\big(2\{u[s_o + (2p+2)\beta_+][s_h - (2p+2)\beta_-]\}^{1/2}\big) \tag{17}$$

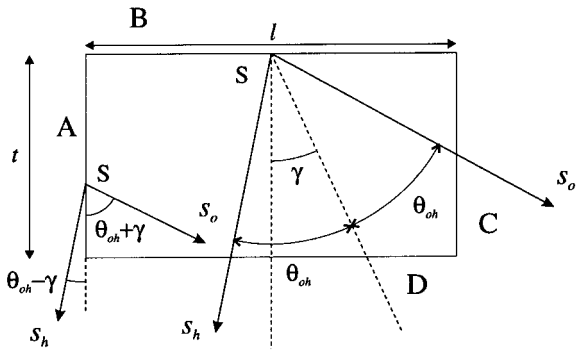

Fig. 1. Crystal dimensions and surface labels. Entrance surfaces are *A* and *B*, exit surfaces *A* and *D*. The angle between $\mathbf{s}_o$ and $\mathbf{s}_h$ is $2\theta_{oh}$. The asymmetry angle γ is measured with respect to the inward normal to the *B* surface. The figure shows the case of positive γ.

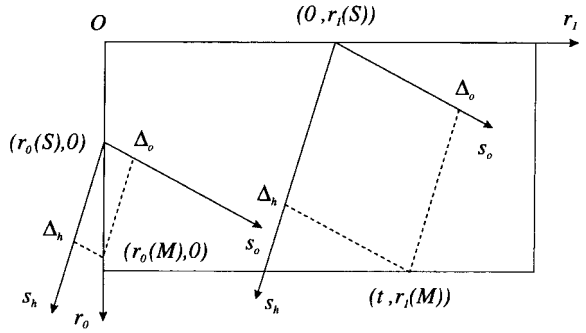

Fig. 2. Coordinate systems used. (r_0, r_1) with origin at the corner *O* are global coordinates, while (s_o, s_h) with origin at the actual source point, *S*, on the *A* or *B* surface are local coordinates.

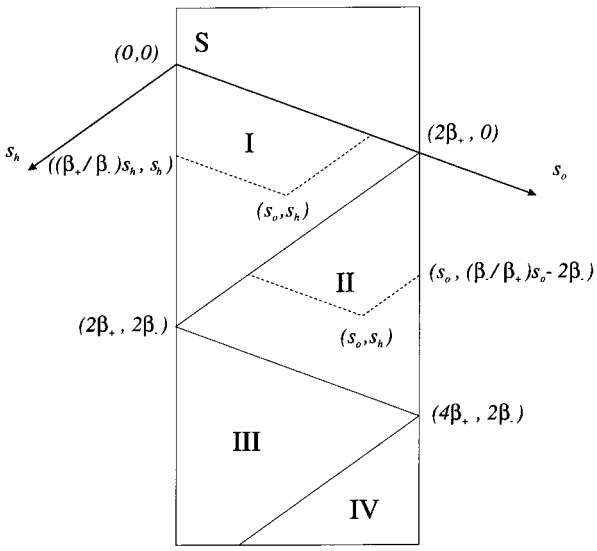

Fig. 3. Region structure when the source *S* is located on the surface *A*. All coordinates are measured in the characteristic length ℓ.

Table 3. *Defining integral operators for the Laue family, $r = \mathsf{L}$, $p = 0, 1, \ldots$*

Region	p	$\mathcal{L}_{oh}$	$\mathcal{L}_{ho}$
$m = 3p+1$	Odd	$\int_{\beta_+[(p+1)-c]}^{s_o} \mathrm{d}s'_o$	$\int_{\beta_-[(p-1)+c]}^{s_h} \mathrm{d}s'_h$
	Even	$\int_{\beta_+ p}^{s_o} \mathrm{d}s'_o$	$\int_{\beta_- p}^{s_h} \mathrm{d}s'_h$
$m = 3p+2$	Odd	$\int_{(\beta_+/\beta_-)s_h-\beta_+ c}^{s_o} \mathrm{d}s'_o$	$\int_{\beta_-(p+1)}^{s_h} \mathrm{d}s'_h$
	Even	$\int_{(\beta_+/\beta_-)s_h-\beta_+ c}^{s_o} \mathrm{d}s'_o$	$\int_{\beta_-(p+c)}^{s_h} \mathrm{d}s'_h$
$m = 3p+3$	Odd	$\int_{\beta_+(p+1)}^{s_o} \mathrm{d}s'_o$	$\int_{(\beta_-/\beta_+)s_o-\beta_-(2-c)}^{s_h} \mathrm{d}s'_h$
	Even	$\int_{\beta_+[(p+2)-c]}^{s_o} \mathrm{d}s'_o$	$\int_{(\beta_-/\beta_+)s_o-\beta_-(2-c)}^{s_h} \mathrm{d}s'_h$

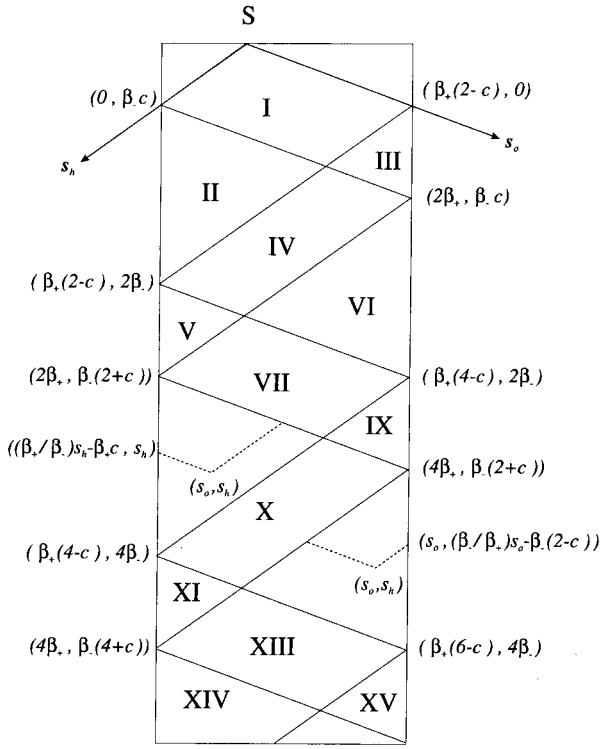

Fig. 4. Region structure when the source S is located on the surface B. All coordinates are measured in the characteristic length ℓ. This implies that $c = 2r_1(S)/l$.

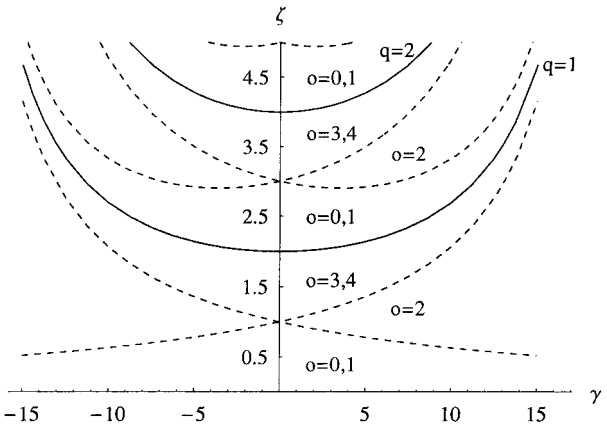

Fig. 5. Different sections in ζ as a function of γ. The figure is drawn with $2\theta_{oh} = 40°$.

$$w(s_o, s_h|6p+6; \mathsf{L}) = (-1)^{p+1}\left[\frac{\beta_-}{\beta_+}\frac{s_o-(2p+2)\beta_+}{s_h+(2p+2)\beta_-}\right]^{p+1} \times J_{2p+2}\left(2\{u[s_o-(2p+2)\beta_+][s_h+(2p+2)\beta_-]\}^{1/2}\right) \tag{18}$$

$$w(s_o, s_h|2p+1; \mathsf{B}) = (-1)^{p}\left[\frac{\beta_+}{\beta_-}\frac{s_h-2p\beta_-}{s_o+2p\beta_+}\right]^{p+1} \times J_{2p+2}\left(2\{u(s_o+2p\beta_+)(s_h-2p\beta_-)\}^{1/2}\right) + (-1)^{p}\left[\frac{\beta_+}{\beta_-}\frac{s_h-2p\beta_-}{s_o+2p\beta_+}\right]^{p} \times J_{2p}\left(2\{u(s_o+2p\beta_+)(s_h-2p\beta_-)\}^{1/2}\right) \tag{19}$$

$$w(s_o, s_h|2p+2; \mathsf{B}) = (-1)^{p+1}\left[\frac{\beta_-}{\beta_+}\frac{s_o-(2p+2)\beta_+}{s_h+(2p+2)\beta_-}\right]^{p+1} \times J_{2p+2}\left(2\{u[s_o-(2p+2)\beta_+][s_h+(2p+2)\beta_-]\}^{1/2}\right) + (-1)^{p+1}\left[\frac{\beta_-}{\beta_+}\frac{s_o-(2p+2)\beta_+}{s_h+(2p+2)\beta_-}\right]^{p} \times J_{2p}\left(2\{u[s_o-(2p+2)\beta_+][s_h+(2p+2)\beta_-]\}^{1/2}\right). \tag{20}$$

2.4. *Integration structure*

In Appendix B, we have summarized in detail the relations that are used to deduce the actual structure for the surface integrations. The integration set-up is not exactly equivalent to the symmetrical case. As before, the integration limits depend on the value of ζ, and we specify 'coarse' intervals in ζ by the integer q in this case defined by

$$q = \mathrm{Int}[\zeta/(\beta_+/\delta_+ + \beta_-/\delta_-)]. \tag{21}$$

It is also necessary to specify subsections within each q interval. These sections are linked to the value of the parameter η, $\eta \in (0, \beta_+/\delta_+ + \beta_-/\delta_-)$, defined by

Table 4. *Relations between exit and entrance surface integration; A–A scattering, region $m = 2p + 1$, $p = 0, 1, \ldots$*

$\zeta = (t/l)\tan\theta_{oh}$

$\big(p(\beta_+/\delta_+) + p(\beta_-/\delta_-), (p+1)(\beta_+/\delta_+) + (p+1)(\beta_-/\delta_-)\big)$

$\big((p+1)(\beta_+/\delta_+) + (p+1)(\beta_-/\delta_-), \infty\big)$

I	y	x
1	$(2p\beta_+, \zeta/\beta_-)$	$\big(2p\beta_-, (\beta_-/\beta_+)y\big)$
2*a*	$\big(2p\beta_+, 2(p+1)\beta_+\big)$	$\big(2p\beta_-, (\beta_-/\beta_+)y\big)$
2*b*	$\big(2(p+1)\beta_+, \zeta/\beta_-\big)$	$\big(2p\beta_-, 2(p+1)\beta_-\big)$

$$\eta = \zeta - q(\beta_+/\delta_+ + \beta_-/\delta_-).$$

Using o for labelling, we arrive at the following scheme:†

$$o = 0 \qquad 0 \le \eta < \frac{1}{2\delta_+\delta_-}$$

$$o = 1 \qquad \frac{1}{2\delta_+\delta_-} \le \eta < \frac{\beta_+}{\delta_+}$$

$$o = 2 \qquad \frac{\beta_+}{\delta_+} \le \eta < \frac{\beta_-}{\delta_-}$$

$$o = 3 \qquad \frac{\beta_-}{\delta_-} \le \eta < \frac{\beta_+}{\delta_+} + \frac{\beta_-}{\delta_-} - \frac{1}{2\delta_+\delta_-}$$

$$o = 4 \quad \frac{\beta_+}{\delta_+} + \frac{\beta_-}{\delta_-} - \frac{1}{2\delta_+\delta_-} \le \eta < \frac{\beta_+}{\delta_+} + \frac{\beta_-}{\delta_-}.$$

An example of the division of a given range in ζ as a function of the asymmetry angle γ is shown in Fig. 5. Since the β and δ parameters depend on θ_{oh}, the Bragg angle becomes a parameter for these kinds of plots. The section limits are closely linked to the surface integration structure. The buildup of contributions to the diffracted fields at the exit surfaces is shown in Figs. 6–8. It is too comprehensive to list the actual integration setup for every scattering mode. A full account is given by Thorkildsen & Larsen (1997). In Tables 4 and 5, we have however included the general results for *A–A* scattering and the results for *B–D* scattering for the special case $q = 0$, $o = 0, 1$. These results are important for a discussion regarding the limits of Laue and Bragg scattering for semi-infinite crystal plates. The two integration schemes, $o = 0$ and $o = 1$, for *B–D* scattering give the same result. This is a general feature independent of the value of q. It also applies to the sections $o = 3$ and $o = 4$.

The extended 'volume' that is used to check the integration setup is shown in Fig. 9. It has the value

$$v' = 2\zeta(1 + \zeta/4\beta_+\beta_-)\ell^2 \sin 2\theta_{oh}. \qquad (22)$$

3. Results

In general, the effect of the asymmetry is to reduce both the value of the extinction factor and the absorption factor, owing to an increase in the mean path lengths of the beams through the crystal. The size of the effect increases with ζ. All results are invariant with respect to a change in the sign of γ, *cf.* Wilkins (1981).

3.1. *Series expansion of the primary extinction factor*

The primary extinction factor is expressed by

$$y_p = y_p(\zeta, \theta_{oh}, \gamma|\xi) = \sum_{n=0}^{\infty}(-1)^n f_n(\zeta, \theta_{oh}, \gamma)\xi^n \qquad (23)$$

with expansion parameter

$$\xi = (t/2\Lambda_{oh}\cos\theta_{oh})^2. \qquad (24)$$

The contributions to the kinematical term, $f_0 = 1$, as functions of ζ are given in Table 6 and are shown in Fig. 10 in the case of $2\theta_{oh} = 40^\circ$. There is a change in the relative weight of the four different scattering terms. Generally, the mixed Bragg–Laue scattering terms become more important with increasing γ. Furthermore, we find that

$$f_0^{A-D}(\gamma) = f_0^{B-A}(-\gamma),$$

which is obvious owing to symmetry reasons.

The first-order coefficients, here given for the case of $\gamma \ge 0$, are

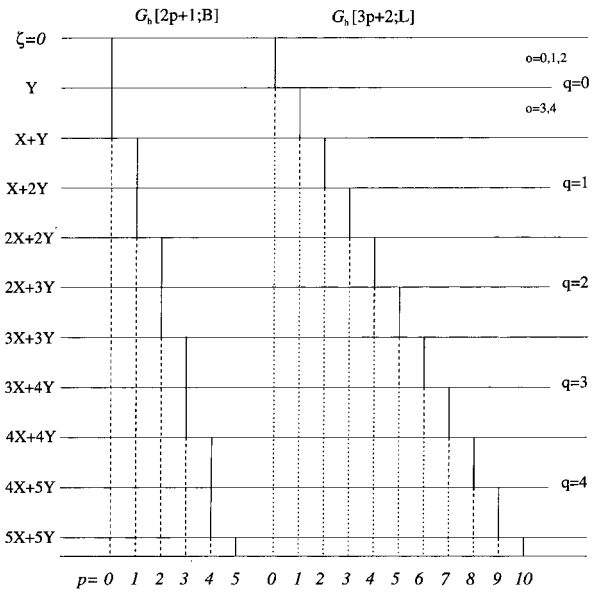

Fig. 6. Contributions to the field at the exit surface *A*. $X = \beta_+/\delta_+$, $Y = \beta_-/\delta_-$, $\gamma \ge 0$.

† This scheme applies to the case $\gamma \ge 0$, then $\beta_+/\delta_+ \le \beta_-/\delta_-$.

Table 5. *Relations between exit and entrance surface integration*

B–D scattering, region $m = 1$, sections $q = 0$, $o = 0, 1$. In these cases, the surface integration consists of three terms: 1*a*, 1*b* and 1*c* ($o = 1$).

$\zeta = (t/l)\tan\theta_{oh}$	I	y	x
$(0, 1/2\delta_+\delta_-)$	1*a*	$(0, (\delta_+/\beta_+\delta_-)\zeta)$	$(2\delta_-\zeta - 2(\beta_+\delta_-^2/\delta_+)y, 2\delta_-\zeta)$
	1*b*	$((\delta_+/\beta_+\delta_-)\zeta, (1/\delta_-) - (\zeta/\beta_-))$	$(0, 2\delta_-\zeta)$
	1*c*	$((1/\delta_-) - (\zeta/\beta_-), (1/\delta_-))$	$(0, 2\beta_-(1 - \delta_- y))$
$(1/2\delta_+\delta_-, \beta_+/\delta_+)$	2*a*	$(0, 1/\delta_- - \zeta/\beta_-)$	$(2\delta_-\zeta - 2(\beta_+\delta_-^2/\delta_+)y, 2\delta_-\zeta)$
	2*b*	$(1/\delta_- - \zeta/\beta_-, (\delta_+/\beta_+\delta_-)\zeta)$	$(2\delta_-\zeta - 2(\beta_+\delta_-^2/\delta_+)y, 2\beta_-(1 - \delta_- y))$
	2*c*	$((\delta_+/\beta_+\delta_-)\zeta, 1/\delta_-)$	$(0, 2\beta_-(1 - \delta_- y))$

$$f_1 = \begin{cases} \frac{4}{3}\delta_+\delta_-(1 - \frac{1}{2}\delta_+\delta_-\zeta) \\ \qquad \text{when } 0 \le \zeta \le \beta_+/\delta_+ \\ \dfrac{[2 - (\beta_+/\delta_+)(1/\zeta)]^2 - 2 + [2 - (\delta_-/\beta_-)\zeta]^2}{6(1/\beta_+\delta_- - 1)\zeta} \\ \qquad \text{when } \beta_+/\delta_+ \le \zeta \le \beta_-/\delta_- \\ \frac{4}{3}\beta_+\beta_-(1 - \frac{1}{2}\beta_+\beta_-\zeta)/\zeta^3 \\ \qquad \text{when } \zeta \ge \beta_-/\delta_- \end{cases} . \tag{25}$$

The coefficients f_n for $n = 1, 2, 3$ are shown as functions of ζ in Fig. 11 for the two cases $\gamma = 0^\circ$ and $|\gamma| = 15^\circ$. It is found that an asymptotic expression occurs for the coefficient f_n when

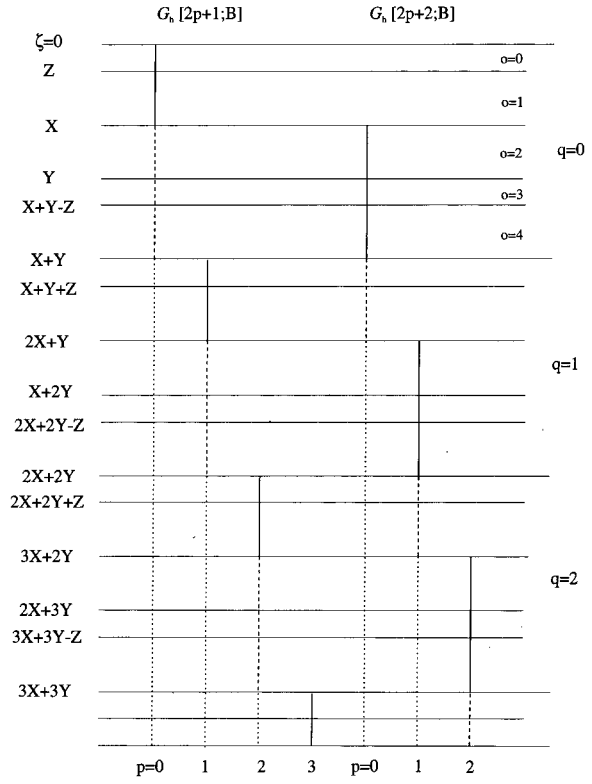

Fig. 7. Contributions to the field at the exit surface *D* from sources on the surface *A*. $X = \beta_+/\delta_+$, $Y = \beta_-/\delta_-$, $Z = 1/(2\delta_+\delta_-)$, $\gamma \ge 0$.

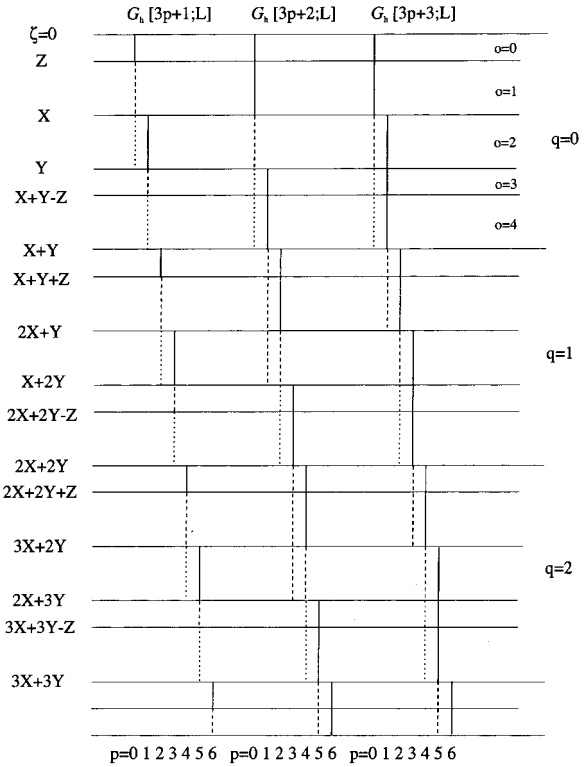

Fig. 8. Contributions to the field at the exit surface *D* from sources on the surface *B*. $X = \beta_+/\delta_+$, $Y = \beta_-/\delta_-$, $Z = 1/2\delta_+\delta_-$, $\gamma \ge 0$.

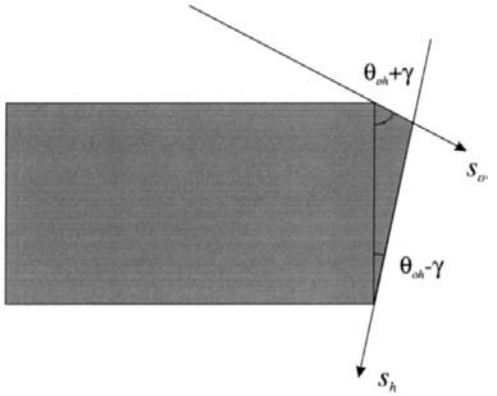

Fig. 9. Extended volume, v', in the case of nonsymmetrical scattering.

Table 6. *Analytical expressions for the contributions to f_0 from the various scattering modes in different sections of ζ, $\gamma \geq 0$*

Scattering	$\zeta \leq \beta_+/\delta_+$	$\beta_+/\delta_+ \leq \zeta \leq \beta_-/\delta_-$	$\beta_-/\delta_- \leq \zeta \leq \beta_+/\delta_+ + \beta_-/\delta_-$	$\zeta \geq \beta_+/\delta_+ + \beta_-/\delta_-$
A–A	$(1/4\beta_+\beta_-)\zeta$	$(1/4\beta_+\beta_-)\zeta$	$(1/4\beta_+\beta_-)\zeta$	$1 - \beta_+\beta_-(1/\zeta)$
B–A	$(\delta_-/4\beta_-^2\delta_+)\zeta$	$(\delta_-/4\beta_-^2\delta_+)\zeta$	$1 - (\beta_-/2\delta_-)(1/\zeta) - (1/4\beta_+\beta_-)\zeta$	$(\beta_+/2\delta_+)(1/\zeta)$
A–D	$(\delta_+/4\beta_+^2\delta_-)\zeta$	$1 - (\beta_+/2\delta_+)(1/\zeta) - (1/4\beta_+\beta_-)\zeta$	$1 - (\beta_+/2\delta_+)(1/\zeta) - (1/4\beta_+\beta_-)\zeta$	$(\beta_-/2\delta_-)(1/\zeta)$
B–D	$1 - (\delta_+\delta_- - 1/4\beta_+\beta_-)\zeta$	$(\beta_+/2\delta_+)(1/\zeta) - (\delta_-/4\beta_-^2\delta_+)\zeta$	$-1 + \beta_+\beta_-(1/\zeta) + (1/4\beta_+\beta_-)\zeta$	0

$$q = n/2, \qquad o = 0 \quad n \text{ an even number}$$
$$q = (n-1)/2, \quad o = 3 \quad n \text{ an odd number}$$

When absorption is included, *i.e.* calculating the generalized extinction factor

$$y = \sum_{n=0}^{\infty} (-1)^n f_n(\zeta, \theta_{oh}, \mu_0, \gamma)\xi^n,$$

we find that the asymptotic level of f_n is reached for

$$q = n + 1, \quad o = 0.$$

Then, by increasing ζ, no contributions to that particular scattering order is added to the diffracted field at the exit.

Examination of the contribution to the expansion coefficients from *A–A* scattering in the limit $\zeta \to \infty$ gives the series for the primary extinction in the Bragg limit for a semi-infinite crystal:

$$\begin{aligned} y_p &= 1 - \tfrac{1}{3}\xi_B + \tfrac{2}{15}\xi_B^2 - \tfrac{17}{315}\xi_B^3 + \ldots \\ &= \tanh(\xi_B)^{1/2}/(\xi_B)^{1/2} \end{aligned} \tag{26}$$

with

$$\xi_B = 4\beta_+\beta_-\xi/\zeta^2 = (l/\Lambda_{oh})^2[\sin(\theta_{oh} + \gamma)\sin(\theta_{oh} - \gamma)]^{-1}. \tag{27}$$

In the same manner, examination of the *B–D* scattering terms in the limit $\zeta \to 0$ gives the Laue limit for the primary extinction in a semi-infinite crystal:†

$$\begin{aligned} y_p &= 1 - \tfrac{1}{3}\xi_L + \tfrac{1}{20}\xi_L^2 - \tfrac{1}{252}\xi_L^3 + \ldots \\ &= [1/(\xi_L)^{1/2}] \sum_n J_{2n+1}[2(\xi_L)^{1/2}] \\ &= {}_1F_2(\tfrac{1}{2}; 1, \tfrac{3}{2}; -\xi_L) \end{aligned} \tag{28}$$

with

$$\xi_L = 4\delta_+\delta_-\xi = (t/\Lambda_{oh})^2[\cos(\theta_{oh} + \gamma)\cos(\theta_{oh} - \gamma)]^{-1}. \tag{29}$$

3.2. *Normal absorption factor*

Analytical expressions for the absorption factor are obtained by using equation (2). Different expressions apply to the ζ ranges: $0 \leq \zeta \leq \beta_+/\delta_+$, $\beta_+/\delta_+ \leq \zeta \leq \beta_-/\delta_-$, $\beta_-/\delta_- \leq \zeta \leq \beta_+/\delta_+ + \beta_-/\delta_-$ and $\zeta \geq \beta_+/\delta_+ + \beta_-/\delta_-$. They are included in Appendix *C*.

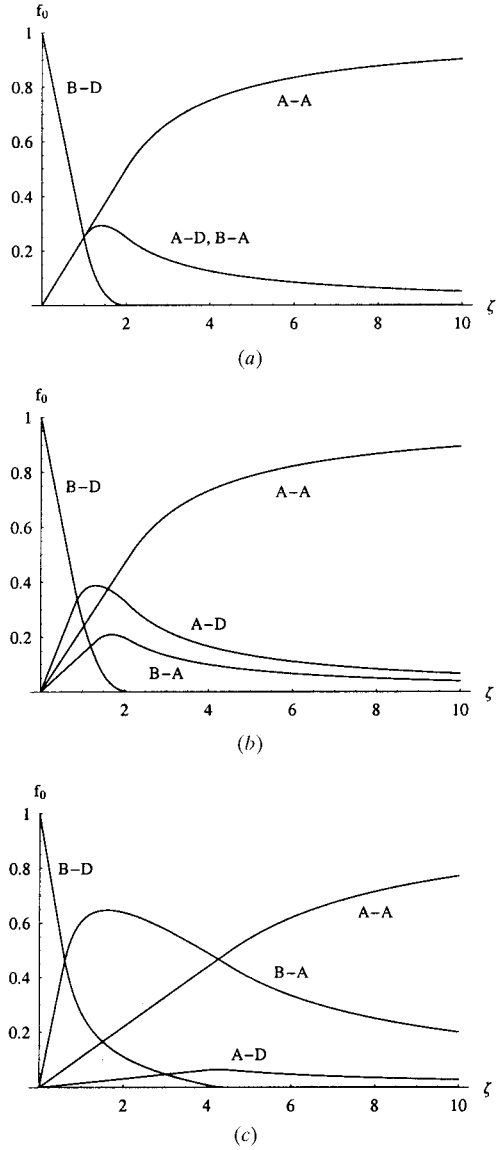

Fig. 10. Buildup of the kinematical level from the various scattering modes. (*a*) $\gamma = 0°$, (*b*) $\gamma = 5°$, (*c*) $\gamma = -15°$. $2\theta_{oh} = 40°$. The reference curves in (*a*) are independent of $2\theta_{oh}$. The *B–A* and *A–D* curves are interchanged when γ changes sign.

† J denotes a Bessel function, F a generalized hypergeometric function.

In Fig. 12, we have shown the range of values for the normal absorption factor obtained by varying γ, $|\gamma| \in (0, 20^\circ)$. In the figure, $2\theta_{oh} = 40^\circ$ and the absorption factor is plotted against ζ for the cases $\mu_0 = \{0.1, 0.5\}$. Three γ profiles are shown for $\mu_0 = 0.5$ in Fig. 13. We observe that the effect of varying γ is almost negligible when $\zeta \leq 1$ and $\mu_0 \lesssim 0.1$.

The normal absorption factor in the Laue limit, A_L, for a semi-infinite crystal, is obtained from the B–D scattering contribution $I = 1b$, region $m = 1$, in the limit $\zeta \to 0$, *cf.* Table 5:

$$A_L = \frac{\exp(-2\delta_+\mu_0\zeta) - \exp(-2\delta_-\mu_0\zeta)}{2(\delta_- - \delta_+)\mu_0\zeta}. \qquad (30)$$

Similarly, the Bragg limit, A_B, results from an analysis of the A–A scattering contribution to absorption in the limit $\zeta \to \infty$. This corresponds to the term $I = 2a$ of Table 4 with $m = 1$ ($p = 0$).

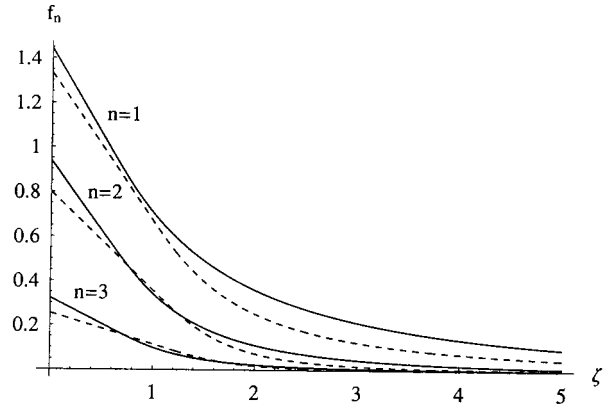

Fig. 11. Extinction coefficients f_1, f_2, f_3 as functions of ζ. $2\theta_{oh} = 40^\circ$. Solid lines: $|\gamma| = 15^\circ$. Dashed lines give the reference at $\gamma = 0^\circ$.

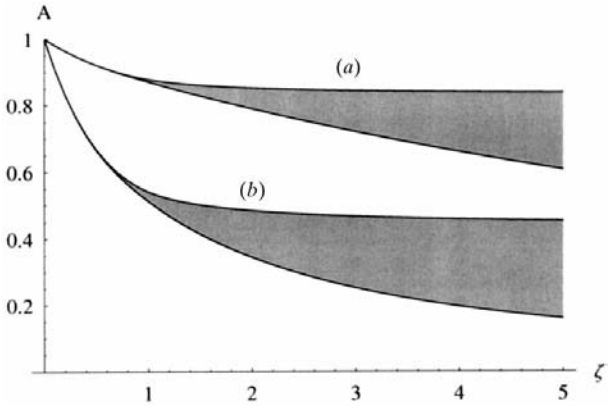

Fig. 12. Range of values for the normal absorption factor. $2\theta_{oh} = 40^\circ$ and $|\gamma| \in (0, 20^\circ)$. (*a*) $\mu_0 = 0.1$, (*b*) $\mu_0 = 0.5$.

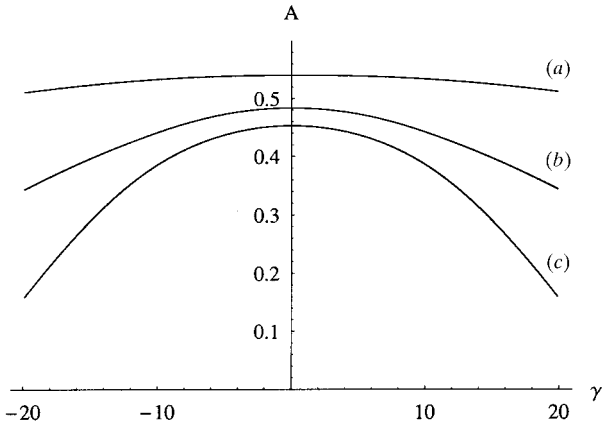

Fig. 13. Variation of the normal absorption factor with γ. $2\theta_{oh} = 40^\circ$, $\mu_0 = 0.5$. (*a*) $\zeta = 1$, (*b*) $\zeta = 2$, (*c*) $\zeta = 5$.

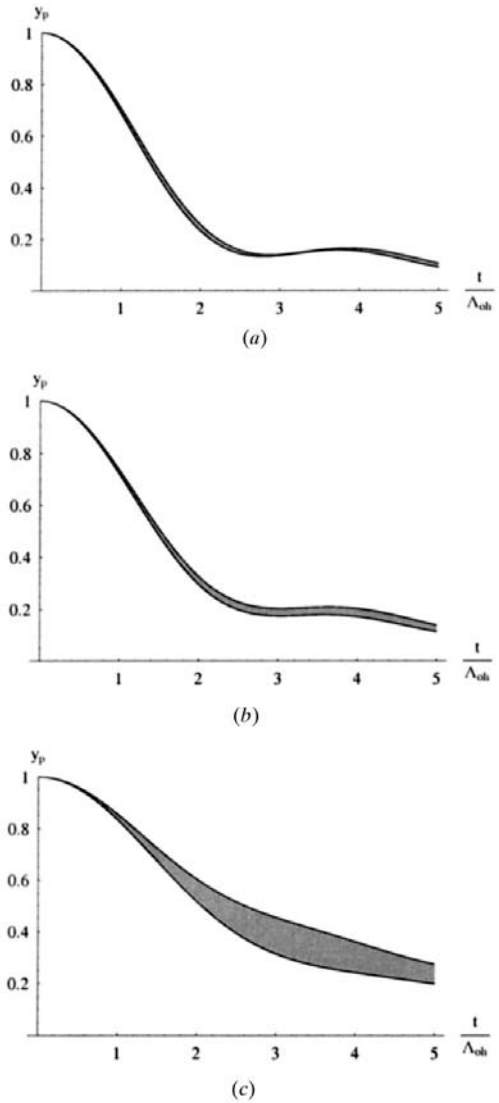

Fig. 14. Range of values for the primary extinction factor as a function of t/Λ_{oh}. (*a*) $t/l = 0.25$, (*b*) $t/l = 1$, (*c*) $t/l = 4$. $2\theta_{oh} = 30^\circ$; $|\gamma| \in (0, 15^\circ)$.

$$A_B = \frac{1 - \exp[-2(\beta_+ + \beta_-)\mu_0]}{2(\beta_+ + \beta_-)\mu_0}. \quad (31)$$

These results are in agreement with those given by Maslen (1995).

3.3. *Numerical results for the primary and generalized extinction factor*

In Fig. 14, we show the range of primary extinction factors spanned by varying the asymmetry angle $|\gamma| \in (0, 15^\circ)$. In the figures $2\theta_{oh} = 30^\circ$ and the extinction factor is plotted against t/Λ_{oh} for the cases $t/l = \{0.25, 1, 4\}$. The results are obtained by performing the surface integrations numerically using the closed expressions for the boundary-value Green functions. We observe that the effect of increasing $|\gamma|$ becomes more pronounced for larger values of t/l. Fig. 15 gives the actual γ profiles for the three cases when $t/\Lambda_{oh} = 2$.

In Fig. 16, we have shown a result for the generalized extinction factor when normal absorption is included in the calculation. Here $t/l = 4$, $2\theta_{oh} = 40^\circ$, $\mu_0 = 0.2$ and $|\gamma| \in (0, 20^\circ)$.

4. Conclusions

The case of nonsymmetrical scattering in a rectangular $t \times l$ crystal adds no topological changes to the Laue and Bragg region geometry and can be dealt with using the same approach as for the symmetrical case. The additional degree of freedom added to the problem is primarily a geometrical one leading to a more complex integration set-up.

The effect of the asymmetry on both extinction and absorption increases with the values of ζ and γ since the geometrical changes of the surface integrations then become more pronounced.

Combining the approach using series expansions with numerical calculations based on the work of Uragami (1971) extends the range of applicability of the method. In the limit of a semi-infinite crystal plate, the results from fundamental dynamical theory are reproduced (Zachariasen, 1945).

A number of details had to be omitted in this presentation, they are fully covered in a report on two-beam diffraction in perfect crystals (Thorkildsen & Larsen, 1997), which is available from the authors on request.

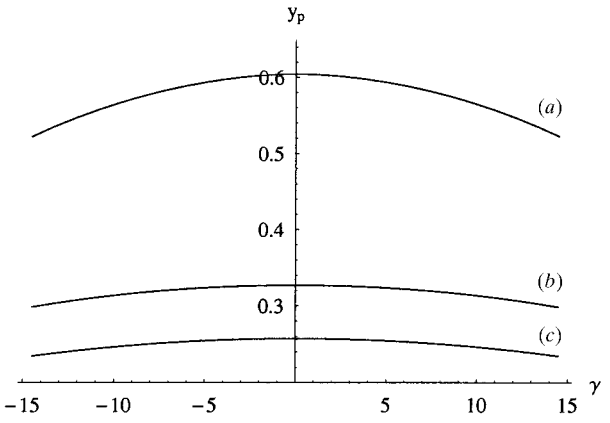

Fig. 15. Variation of the primary extinction factor with γ. $2\theta_{oh} = 30^\circ$, $t/\Lambda_{oh} = 2$. (*a*) $t/l = 4$, (*b*) $t/l = 1$, (*c*) $t/l = 0.25$.

APPENDIX *A*

Here we explore some geometrical aspects. To simplify the reading, we have not scaled the geometrical quantities to the characteristic length ℓ.

*A*1. *Coordinate systems*

With the origin of the local coordinate system on the entrance surface A, the relation between the local (s_o, s_h) and the global (r_0, r_1) coordinates for a general point within the crystal is given by

$$\begin{aligned} s_o &= \frac{\sin(\theta_{oh} - \gamma)}{\sin 2\theta_{oh}}[r_0 - r_0(S)] + \frac{\cos(\theta_{oh} - \gamma)}{\sin 2\theta_{oh}} r_1 \\ s_h &= \frac{\sin(\theta_{oh} + \gamma)}{\sin 2\theta_{oh}}[r_0 - r_0(S)] - \frac{\cos(\theta_{oh} + \gamma)}{\sin 2\theta_{oh}} r_1. \end{aligned} \quad (32)$$

With the origin of the local coordinate system on the entrance surface B, the relation between the local and global coordinates for a general point is given by

$$\begin{aligned} s_o &= \frac{\sin(\theta_{oh} - \gamma)}{\sin 2\theta_{oh}} r_0 + \frac{\cos(\theta_{oh} - \gamma)}{\sin 2\theta_{oh}}[r_1 - r_1(S)] \\ s_h &= \frac{\sin(\theta_{oh} + \gamma)}{\sin 2\theta_{oh}} r_0 - \frac{\cos(\theta_{oh} + \gamma)}{\sin 2\theta_{oh}}[r_1 - r_1(S)] \end{aligned}. \quad (33)$$

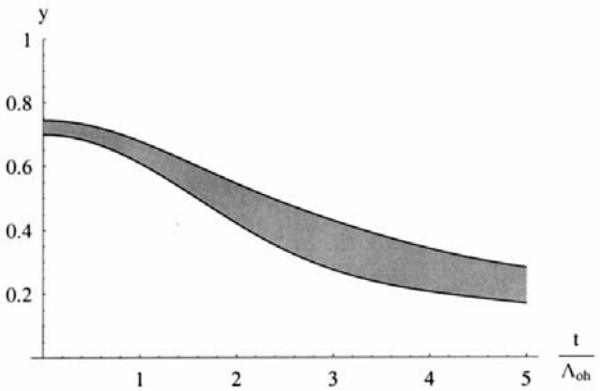

Fig. 16. Range of values for the generalized extinction factor as a function of t/Λ_{oh}, $t/l = 4$, $2\theta_{oh} = 40^\circ$, $\mu_0 = 0.2$, $|\gamma| \in (0, 20^\circ)$. Upper limit corresponds to $\gamma = 0^\circ$, lower limit to $|\gamma| = 20^\circ$. Since the crystal has a nonvanishing size, the limit $t/\Lambda_{oh} \to 0$ corresponds to $\Lambda_{oh} \to \infty$.

Table 7. *Coordinates for a point M on an exit surface in relation to a source point S*

Surfaces	Δ_o	Δ_h
A–A	$[\sin(\theta_{oh}-\gamma)/\sin 2\theta_{oh}][r_o(M)-r_o(S)]$	$[\sin(\theta_{oh}+\gamma)/\sin 2\theta_{oh}][r_o(M)-r_o(S)]$
A–D	$\left[\frac{\sin(\theta_{oh}-\gamma)}{\sin 2\theta_{oh}}\right][t-r_o(S)]+\left[\frac{\cos(\theta_{oh}-\gamma)}{\sin 2\theta_{oh}}\right]r_1(M)$	$\left[\frac{\sin(\theta_{oh}+\gamma)}{\sin 2\theta_{oh}}\right][t-r_o(S)]-\left[\frac{\cos(\theta_{oh}+\gamma)}{\sin 2\theta_{oh}}\right]r_1(M)$
B–A	$\left[\frac{\sin(\theta_{oh}-\gamma)}{\sin 2\theta_{oh}}\right]r_o(M)-\left[\frac{\cos(\theta_{oh}-\gamma)}{\sin 2\theta_{oh}}\right]r_1(S)$	$\left[\frac{\sin(\theta_{oh}+\gamma)}{\sin 2\theta_{oh}}\right]r_o(M)+\left[\frac{\cos(\theta_{oh}+\gamma)}{\sin 2\theta_{oh}}\right]r_1(S)$
B–D	$\left[\frac{\sin(\theta_{oh}-\gamma)}{\sin 2\theta_{oh}}\right]t+\left[\frac{\cos(\theta_{oh}-\gamma)}{\sin 2\theta_{oh}}\right][(r_1(M)-r_1(S)]$	$\left[\frac{\sin(\theta_{oh}+\gamma)}{\sin 2\theta_{oh}}\right]t-\left[\frac{\cos(\theta_{oh}+\gamma)}{\sin 2\theta_{oh}}\right][r_1(M)-r_1(S)]$

Table 8. *Change of variables – definitions*

Surfaces	Entrance	Exit
A–A	$r_0(S)=r_0(M)-2\beta_+\cos\theta_{oh}\,x$	$r_0(M)=2\beta_-\cos\theta_{oh}\,y$
A–D	$r_0(S)=t-(\beta_+/\delta_+)[r_1(M)/\tan\theta_{oh}]-2\beta_+\cos\theta_{oh}\,x$	$r_1(M)=2\delta_-\sin\theta_{oh}\,y$
B–A	$r_1(S)=2\delta_+\sin\theta_{oh}\,x-(\delta_+/\delta_-)r_0(M)\tan\theta_{oh}$	$r_0(M)=2\beta_-\cos\theta_{oh}\,y$
B–D	$r_1(S)=2\delta_+\sin\theta_{oh}\,x+r_1(M)-(\delta_+/\beta_+)t\tan\theta_{oh}$	$r_1(M)=2\delta_-\sin\theta_{oh}\,y$

Table 9. *Coordinate limits for the different regions in the crystal with source point S on entrance surface A, $p = 0, 1, \ldots$*

Region	Limits in s_o	Limits in s_h
$m=2p+1$	$\big(2p\beta_+(l/2\sin\theta_{oh}),\,2(p+1)\beta_+(l/2\sin\theta_{oh})\big)$	$\big(2p\beta_-(l/2\sin\theta_{oh}),\,2(p+1)\beta_-(l/2\sin\theta_{oh})\big)$
$m=2p+2$	$\big(2(p+1)\beta_+(l/2\sin\theta_{oh}),\,2(p+2)\beta_+(l/2\sin\theta_{oh})\big)$	$\big(2p\beta_-(l/2\sin\theta_{oh}),\,2(p+1)\beta_-(l/2\sin\theta_{oh})\big)$

Table 10. *Coordinate limits for the different regions in the crystal with source point S on entrance surface B, $p = 0, 1, \ldots$*

Region	p	Limits in s_o	Limits in s_h
$m=3p+1$	Odd	$\beta_+\big((p+1)(l/2\sin\theta_{oh})-[r_1(S)/\sin\theta_{oh}],\,(p+1)(l/2\sin\theta_{oh})\big)$	$\beta_-\big((p-1)(l/2\sin\theta_{oh})+[r_1(S)/\sin\theta_{oh}],\,(p+1)(l/2\sin\theta_{oh})\big)$
	Even	$\beta_+\big(p(l/2\sin\theta_{oh}),\,(p+2)(l/2\sin\theta_{oh})-[r_1(S)/\sin\theta_{oh}]\big)$	$\beta_-\big(p(l/2\sin\theta_{oh}),\,p(l/2\sin\theta_{oh})+[r_1(S)/\sin\theta_{oh}]\big)$
$m=3p+2$	Odd	$\beta_+\big((p+1)(l/2\sin\theta_{oh})-[r_1(S)/\sin\theta_{oh}],\,(p+1)(l/2\sin\theta_{oh})\big)$	$\beta_-\big((p+1)(l/2\sin\theta_{oh}),\,(p+1)(l/2\sin\theta_{oh})+[r_1(S)/\sin\theta_{oh}]\big)$
	Even	$\beta_+\big(p(l/2\sin\theta_{oh}),\,(p+2)(l/2\sin\theta_{oh})-[r_1(S)/\sin\theta_{oh}]\big)$	$\beta_-\big(p(l/2\sin\theta_{oh})+[r_1(S)/\sin\theta_{oh}],\,(p+2)(l/2\sin\theta_{oh})\big)$
$m=3p+3$	Odd	$\beta_+\big((p+1)(l/2\sin\theta_{oh}),\,(p+3)(l/2\sin\theta_{oh})-[r_1(S)/\sin\theta_{oh}]\big)$	$\beta_-\big((p-1)(l/2\sin\theta_{oh})+[r_1(S)/\sin\theta_{oh}],\,(p+1)(l/2\sin\theta_{oh})\big)$
	Even	$\beta_+\big((p+2)(l/2\sin\theta_{oh})-[r_1(S)/\sin\theta_{oh}],\,(p+2)(l/2\sin\theta_{oh})\big)$	$\beta_-\big(p(l/2\sin\theta_{oh}),\,p(l/2\sin\theta_{oh})+[r_1(S)/\sin\theta_{oh}]\big)$

*A*2. *Coordinates for an exit point M*

It is convenient to represent an exit point M in the (r_0, r_1) coordinate system. On exit surface A, $r_0(M) \in (0, t)$ and $r_1(M) = 0$, while, on exit surface D, $r_0(M) = t$ and $r_1(M) \in (0, l)$. The coordinates for an exit point with respect to the appropriate source point, *i.e.* Δ_o and Δ_h, are given in Table 7.

*A*3. *Definition of new variables*

The surface integrations are simplified by introducing a set of variables, (x, y), with somewhat different definitions according to the actual combination of entrance and exit surfaces. The definitions are given in Table 8.

APPENDIX *B*
Deducing the integration structure

The coordinate limits for a general point, expressed in (s_o, s_h), for a given region, m, with source point on A and B, respectively, are given in Tables 9 and 10. Combining these restrictions with the expressions for Δ_o and Δ_h in Table 7 gives the sets of inequalities listed in Tables 11–14. In addition, the coordinates of the exit points, expressed in (r_0, r_1), must satisfy the conditions: $r_0 \in (0, t)$ and $r_1 \in (0, l)$. The integration structure, *i.e.* the range of possible positions for the source S giving rise to a diffracted field at the exit point M within the region m, together with the range of the possible positions for M, are deduced from these inequalities.

APPENDIX *C*
Expressions for the normal absorption factor

The normal absorption factors for $\gamma \geq 0$ in the four actual ζ intervals are given here. There is an apparent asymmetry in the $\pm$ indices for the range $\beta_+/\delta_+ \leq \zeta \leq \beta_-/\delta_-$, *i.e.* for $o = 2$. This is connected to a change in the integration setup for this section owing to the interchange of β_+/δ_+ and β_-/δ_- when γ changes

Table 11. *Restriction on coordinates for entrance and exit points, A–A scattering*

$0 \le r_0(S) \le t$ and $0 \le r_0(M) \le t$.

Region	Inequalities
$m = 2p+1$	$r_0(M) - 2(p+1)(\beta_+\beta_- l/\tan\theta_{oh}) \le r_0(S) \le r_0(M) - 2p(\beta_+\beta_- l/\tan\theta_{oh})$

Table 12. *Restriction on coordinates for entrance and exit points, A–D scattering*

$0 \le r_0(S) \le t$ and $0 \le r_1(M) \le l$.

Region	Inequalities
$m = 2p+1$	$t + (\beta_-/\delta_-)[r_1(M)/\tan\theta_{oh}] - 2(p+1)(\beta_+\beta_- l/\tan\theta_{oh}) \le r_0(S) \le t + (\beta_-/\delta_-)[r_1(M)/\tan\theta_{oh}] - 2p(\beta_+\beta_- l/\tan\theta_{oh})$
	$t - (\beta_+/\delta_+)[r_1(M)/\tan\theta_{oh}] - 2(p+1)(\beta_+\beta_- l/\tan\theta_{oh}) \le r_0(S) \le t - (\beta_+/\delta_+)[r_1(M)/\tan\theta_{oh}] - 2p(\beta_+\beta_- l/\tan\theta_{oh})$
$m = 2p+2$	$t + (\beta_-/\delta_-)[r_1(M)/\tan\theta_{oh}] - 2(p+2)(\beta_+\beta_- l/\tan\theta_{oh}) \le r_0(S) \le t + (\beta_-/\delta_-)[r_1(M)/\tan\theta_{oh}] - 2(p+1)(\beta_+\beta_- l/\tan\theta_{oh})$
	$t - (\beta_+/\delta_+)[r_1(M)/\tan\theta_{oh}] - 2(p+1)(\beta_+\beta_- l/\tan\theta_{oh}) \le r_0(S) \le t - (\beta_+/\delta_+)[r_1(M)/\tan\theta_{oh}] - 2p(\beta_+\beta_- l/\tan\theta_{oh})$

sign. However, as pointed out in the main text, $A(-|\gamma|) = A(|\gamma|)$.

(i) $\zeta \le \beta_+/\delta_+$:

$$
\begin{aligned}
A = \frac{1}{2\zeta\mu_0}\Bigg(&\frac{1}{(\beta_+ + \beta_-)}\zeta \\
&+ \frac{\beta_+}{2\beta_-\delta_+(\beta_+ + \beta_-)}\frac{1}{\mu_0} \\
&+ \frac{\beta_-}{2\beta_+\delta_-(\beta_+ + \beta_-)}\frac{1}{\mu_0} \\
&- \frac{1}{(\delta_+ - \delta_-)}\exp[-2\delta_+\mu_0\zeta] \\
&+ \frac{1}{(\delta_+ - \delta_-)}\exp[-2\delta_-\mu_0\zeta] \\
&- \frac{1}{2\beta_-(\delta_+ - \delta_-)}\frac{1}{\mu_0}\exp[-2\delta_-\mu_0\zeta] \\
&+ \frac{1}{2\beta_+(\delta_+ - \delta_-)}\frac{1}{\mu_0}\exp[-2\delta_+\mu_0\zeta] \\
&+ \frac{\delta_+}{\beta_+(\delta_+ - \delta_-)}\zeta\exp[-2\delta_+\mu_0\zeta] \\
&- \frac{\delta_-}{\beta_-(\delta_+ - \delta_-)}\zeta\exp[-2\delta_-\mu_0\zeta] \\
&+ \frac{\delta_+}{2\beta_+(\delta_+ - \delta_-)^2}\frac{1}{\mu_0}\exp[-2\delta_+\mu_0\zeta] \\
&+ \frac{\delta_-}{2\beta_-(\delta_+ - \delta_-)^2}\frac{1}{\mu_0}\exp[-2\delta_-\mu_0\zeta] \\
&- \frac{\beta_+\beta_-}{(\beta_+ + \beta_-)^2}\frac{1}{\mu_0}\left\{1 - \exp\left[-\left(\frac{1}{\beta_+} + \frac{1}{\beta_-}\right)\mu_0\zeta\right]\right\} \\
&+ \frac{\beta_+\delta_-}{(\beta_+ + \beta_-)(\delta_+ - \delta_-)}\frac{1}{\mu_0}\exp\left[-\left(\frac{1}{\beta_+} + \frac{1}{\beta_-}\right)\mu_0\zeta\right] \\
&- \frac{\beta_-\delta_+}{(\beta_+ + \beta_-)(\delta_+ - \delta_-)}\frac{1}{\mu_0}\exp\left[-\left(\frac{1}{\beta_+} + \frac{1}{\beta_-}\right)\mu_0\zeta\right] \\
&- \frac{\delta_+\delta_-}{(\delta_+ - \delta_-)^2}\frac{1}{\mu_0}\exp\left[-\left(\frac{1}{\beta_+} + \frac{1}{\beta_-}\right)\mu_0\zeta\right]\Bigg)
\end{aligned}
\tag{34}
$$

(ii) $\beta_+/\delta_+ \le \zeta \le \beta_-/\delta_-$:

$$
\begin{aligned}
A = \frac{1}{2\zeta\mu_0}\Bigg(&\frac{1}{(\beta_+ + \beta_-)}\zeta \\
&+ \frac{\beta_+}{2\beta_-\delta_+(\beta_+ + \beta_-)}\frac{1}{\mu_0} \\
&+ \frac{\beta_-}{2\beta_+\delta_-(\beta_+ + \beta_-)}\frac{1}{\mu_0} \\
&+ \frac{1}{(\delta_+ - \delta_-)}\exp[-2\delta_-\mu_0\zeta] \\
&- \frac{\delta_-}{\beta_-(\delta_+ - \delta_-)}\zeta\exp[-2\delta_-\mu_0\zeta] \\
&- \frac{1}{2\beta_-(\delta_+ - \delta_-)}\frac{1}{\mu_0}\exp[-2\delta_-\mu_0\zeta] \\
&+ \frac{\delta_-}{2\beta_-(\delta_+ - \delta_-)^2}\frac{1}{\mu_0}\exp[-2\delta_-\mu_0\zeta] \\
&- \frac{1}{2\beta_+\delta_-}\frac{1}{\mu_0}\exp[-2\beta_+\mu_0] \\
&- \frac{\beta_+\beta_-}{(\beta_+ + \beta_-)^2}\frac{1}{\mu_0}\left\{1 - \exp\left[-\left(\frac{1}{\beta_+} + \frac{1}{\beta_-}\right)\mu_0\zeta\right]\right\} \\
&+ \frac{\beta_+\delta_-}{(\beta_+ + \beta_-)(\delta_+ - \delta_-)}\frac{1}{\mu_0}\exp\left[-\left(\frac{1}{\beta_+} + \frac{1}{\beta_-}\right)\mu_0\zeta\right] \\
&- \frac{\beta_-\delta_+}{(\beta_+ + \beta_-)(\delta_+ - \delta_-)}\frac{1}{\mu_0}\exp\left[-\left(\frac{1}{\beta_+} + \frac{1}{\beta_-}\right)\mu_0\zeta\right] \\
&- \frac{\delta_+\delta_-}{(\delta_+ - \delta_-)^2}\frac{1}{\mu_0}\exp\left[-\left(\frac{1}{\beta_+} + \frac{1}{\beta_-}\right)\mu_0\zeta\right] \\
&+ \frac{\delta_+}{2\beta_+\delta_-(\delta_+ - \delta_-)}\frac{1}{\mu_0} \\
&\times \exp\left[-2\mu_0\left(\frac{\beta_+}{\delta_+}(\delta_+ - \delta_-) + \delta_-\zeta\right)\right] \\
&+ \frac{\delta_+}{2\beta_+(\delta_+ - \delta_-)^2}\frac{1}{\mu_0} \\
&\times \exp\left[-2\mu_0\left(\frac{\beta_+}{\delta_+}(\delta_+ - \delta_-) + \delta_-\zeta\right)\right]\Bigg)
\end{aligned}
\tag{35}
$$

Table 13. *Restriction on coordinates for entrance and exit points, B–A scattering*

$0 \le r_1(S) \le l$ and $0 \le r_0(M) \le t$.

Region	p	Inequalities
$m = 3p + 2$	Odd	$\beta_+\beta_-[(p+1)l - 2r_1(S)] \le r_0(M)\tan\theta_{oh} - (\beta_-/\delta_-)r_1(S) \le \beta_+\beta_-(p+1)l$ $\beta_+\beta_-(p+1)l \le r_0(M)\tan\theta_{oh} + (\beta_+/\delta_+)r_1(S) \le \beta_+\beta_-[(p+1)l + 2r_1(S)]$
	Even	$\beta_+\beta_-pl \le r_0(M)\tan\theta_{oh} - (\beta_-/\delta_-)r_1(S) \le \beta_+\beta_-[(p+2)l - 2r_1(S)]$ $\beta_+\beta_-[pl + 2r_1(S)] \le r_0(M)\tan\theta_{oh} + (\beta_+/\delta_+)r_1(S) \le (\beta_+\beta_-)(p+2)l$

(iii) $\beta_-/\delta_- \le \zeta \le \beta_+/\delta_+ + \beta_-/\delta_-$:

$$
\begin{aligned}
A = \frac{1}{2\zeta\mu_0}\Bigg(&\frac{1}{(\beta_+ + \beta_-)}\zeta \\
&+ \frac{\beta_+}{2\beta_-\delta_+(\beta_+ + \beta_-)}\frac{1}{\mu_0} \\
&+ \frac{\beta_-}{2\beta_+\delta_-(\beta_+ + \beta_-)}\frac{1}{\mu_0} \\
&- \frac{1}{2\beta_-\delta_+}\frac{1}{\mu_0}\exp[-2\beta_-\mu_0] \\
&- \frac{1}{2\beta_+\delta_-}\frac{1}{\mu_0}\exp[-2\beta_+\mu_0] \\
&- \frac{\beta_+\beta_-}{(\beta_+ + \beta_-)^2}\frac{1}{\mu_0}\left\{1 - \exp\left[-\left(\frac{1}{\beta_+} + \frac{1}{\beta_-}\right)\mu_0\zeta\right]\right\} \\
&+ \frac{\beta_+\delta_-}{(\beta_+ + \beta_-)(\delta_+ - \delta_-)}\frac{1}{\mu_0}\exp\left[-\left(\frac{1}{\beta_+} + \frac{1}{\beta_-}\right)\mu_0\zeta\right] \\
&- \frac{\beta_-\delta_+}{(\beta_+ + \beta_-)(\delta_+ - \delta_-)}\frac{1}{\mu_0}\exp\left[-\left(\frac{1}{\beta_+} + \frac{1}{\beta_-}\right)\mu_0\zeta\right] \\
&- \frac{\delta_+\delta_-}{(\delta_+ - \delta_-)^2}\frac{1}{\mu_0}\exp\left[-\left(\frac{1}{\beta_+} + \frac{1}{\beta_-}\right)\mu_0\zeta\right] \\
&- \frac{\delta_-}{2\beta_-\delta_+(\delta_+ - \delta_-)}\frac{1}{\mu_0} \\
&\times \exp\left[-2\mu_0\left(\frac{\beta_-}{\delta_-}(\delta_- - \delta_+) + \delta_+\zeta\right)\right] \\
&+ \frac{\delta_+}{2\beta_+\delta_-(\delta_+ - \delta_-)}\frac{1}{\mu_0} \\
&\times \exp\left[-2\mu_0\left(\frac{\beta_+}{\delta_+}(\delta_+ - \delta_-) + \delta_-\zeta\right)\right] \\
&+ \frac{\delta_+}{2\beta_+(\delta_+ - \delta_-)^2}\frac{1}{\mu_0} \\
&\times \exp\left[-2\mu_0\left(\frac{\beta_+}{\delta_+}(\delta_+ - \delta_-) + \delta_-\zeta\right)\right] \\
&+ \frac{\delta_-}{2\beta_-(\delta_+ - \delta_-)^2}\frac{1}{\mu_0} \\
&\times \exp\left[-2\mu_0\left(\frac{\beta_-}{\delta_-}(\delta_- - \delta_+) + \delta_+\zeta\right)\right]\Bigg) \qquad (36)
\end{aligned}
$$

(iv) $\zeta \ge \beta_+/\delta_+ + \beta_-/\delta_-$:

$$
\begin{aligned}
A = \frac{1}{2\zeta\mu_0}\Bigg(&\frac{\beta_+}{2\beta_-\delta_+(\beta_+ + \beta_-)}\frac{1}{\mu_0} \\
&+ \frac{\beta_-}{2\beta_+\delta_-(\beta_+ + \beta_-)}\frac{1}{\mu_0} \\
&- \frac{1}{2\beta_+\delta_-}\frac{1}{\mu_0}\exp[-2\beta_+\mu_0] \\
&- \frac{1}{2\beta_-\delta_+}\frac{1}{\mu_0}\exp[-2\beta_-\mu_0] \\
&+ \frac{1}{(\beta_+ + \beta_-)}\zeta\{1 - \exp[-2(\beta_+ + \beta_-)\mu_0]\} \\
&+ \frac{2\beta_+\beta_-}{(\beta_+ + \beta_-)}\exp[-2(\beta_+ + \beta_-)\mu_0] \\
&- \frac{\beta_+\beta_-}{(\beta_+ + \beta_-)^2}\frac{1}{\mu_0}\{1 - \exp[-2(\beta_+ + \beta_-)\mu_0]\} \\
&+ \frac{1}{2(\beta_+ + \beta_-)\delta_+}\frac{1}{\mu_0}\exp[-2\mu_0(\beta_+ + \beta_-)] \\
&+ \frac{1}{2(\beta_+ + \beta_-)\delta_-}\frac{1}{\mu_0}\exp[-2\mu_0(\beta_+ + \beta_-)]\Bigg). \qquad (37)
\end{aligned}
$$

References

Afanasev, A. M. & Melkonyan, M. K. (1983). *Acta Cryst.* A**39**, 207–210.

Authier, A. (1996). *International Tables for Crystallography*, Vol. B, edited by U. Shmueli, pp. 464–480. Dordrecht: Kluwer Academic Publishers.

Becker, P. (1977). *Acta Cryst.* A**33**, 667–671.

Holý, V. (1996). *Proceedings, X-ray and Neutron Dynamical Diffraction. Theory and Applications*, edited by A. Authier, S. Lagomarsino & B. Tanner. *NATO ASI Series Series B: Physics*, Vol. 357, pp. 33–42. New York: Plenum.

Hung, H. H. & Chang, S.-L. (1989). *Acta Cryst.* A**45**, 823–833.

Maslen, E. N. (1995). *International Tables for Crystallography*, Vol. C, edited by A. J. C. Wilson, pp. 520–529. Dordrecht: Kluwer Academic Publishers.

Pinsker, Z. G. (1978). *Dynamical Scattering of X-rays in Crystals.* Berlin: Springer-Verlag.

Table 14. *Restriction on coordinates for entrance and exit points, B–D scattering*

$0 \le r_1(S) \le l$ and $0 \le r_1(M) \le l$.

Region	p	Inequalities
$m = 3p + 1$	Odd	$\beta_+\beta_-[(p+1)l - 2r_1(S)] \le t\tan\theta_{oh} + (\beta_-/\delta_-)[r_1(M) - r_1(S)] \le \beta_+\beta_-(p+1)l$ $\beta_+\beta_-[(p-1)l + 2r_1(S)] \le t\tan\theta_{oh} - (\beta_+/\delta_+)[r_1(M) - r_1(S)] \le \beta_+\beta_-(p+1)l$
	Even	$\beta_+\beta_-pl \le t\tan\theta_{oh} + (\beta_-/\delta_-)[r_1(M) - r_1(S)] \le \beta_+\beta_-[(p+2)l - 2r_1(S)]$ $\beta_+\beta_-pl \le t\tan\theta_{oh} - (\beta_+/\delta_+)[r_1(M) - r_1(S)] \le \beta_+\beta_-[pl + 2r_1(S)]$
$m = 3p + 2$	Odd	$\beta_+\beta_-[(p+1)l - 2r_1(S)] \le t\tan\theta_{oh} + (\beta_-/\delta_-)[r_1(M) - r_1(S)] \le \beta_+\beta_-(p+1)l$ $\beta_+\beta_-(p+1)l \le t\tan\theta_{oh} - (\beta_+/\delta_+)[r_1(M) - r_1(S)] \le \beta_+\beta_-[(p+1)l + 2r_1(S)]$
	Even	$\beta_+\beta_-pl \le t\tan\theta_{oh} + (\beta_-/\delta_-)[r_1(M) - r_1(S)] \le \beta_+\beta_-[(p+2)l - 2r_1(S)]$ $\beta_+\beta_-[pl + 2r_1(S)] \le t\tan\theta_{oh} - (\beta_+/\delta_+)[r_1(M) - r_1(S)] \le \beta_+\beta_-(p+2)l$
$m = 3p + 3$	Odd	$\beta_+\beta_-(p+1)l \le t\tan\theta_{oh} + (\beta_-/\delta_-)[r_1(M) - r_1(S)] \le \beta_+\beta_-[(p+3)l - 2r_1(S)]$ $\beta_+\beta_-[(p-1)l + 2r_1(S)] \le t\tan\theta_{oh} - (\beta_+/\delta_+)[r_1(M) - r_1(S)] \le \beta_+\beta_-(p+1)l$
	Even	$\beta_+\beta_-[(p+2)l - 2r_1(S)] \le t\tan\theta_{oh} + (\beta_-/\delta_-)[r_1(M) - r_1(S)] \le \beta_+\beta_-(p+2)l$ $\beta_+\beta_-pl \le t\tan\theta_{oh} - (\beta_+/\delta_+)[r_1(M) - r_1(S)] \le \beta_+\beta_-[pl + 2r_1(S)]$

Sommerfeld, A. (1949). *Partial Differential Equations.* New York: Academic Press.

Takagi, S. (1962). *Acta Cryst.* **15**, 1311–1312.

Takagi, S. (1969). *J. Phys. Soc. Jpn*, **26**, 1239–1253.

Taupin, D. (1964). *Bull. Soc. Fr. Minéral. Cristallogr.* **87**, 469–511.

Thorkildsen, G. & Larsen, H. B. (1997). *Two Beam Diffraction in Perfect Crystals Analyzed by Takagi's Equations.* Part 1. *Basic Principles and Methods of Solution.* Technical Report 30. Stavanger College, Stavanger, Norway.

Thorkildsen, G. & Larsen, H. B. (1998*a*). *Acta Cryst.* A**54**, 172–185.

Thorkildsen, G. & Larsen, H. B. (1998*b*). *Acta Cryst.* A**54**, 186–190.

Thorkildsen, G. & Larsen, H. B. (1998*c*). *Acta Cryst.* A**54** 416–429.

Uragami, T. S. (1971). *J. Phys. Soc. Jpn*, **31**, 1141–1161.

Wilkins, S. W. (1978). *Proc. R. Soc. London Ser. A*, **364**, 569–589.

Wilkins, S. W. (1981). *Philos. Trans. R. Soc. London*, **299**, 275–317.

Zachariasen, W. H. (1945). *Theory of X-ray Diffraction in Crystals.* London: John Wiley.